Applied Soft Computing

Applied Soft Computing 8 (2008) 1680–1691

Handling of impreciseness in gray level corner detection using fuzzy set theoretic approach

Minakshi Banerjee [1,*], Malay K. Kundu

Machine Intelligence Unit, Center for Soft Computing Research, Indian Statistical Institute, 203, B.T. Road, Kolkata 700108, India

Received 20 March 2007; received in revised form 3 April 2007; accepted 13 September 2007
Available online 12 February 2008

Abstract

Reliable corner detection is an important task in determining shape of different regions in an image. To detect corners in a gray level image under imprecise information, an algorithm based on fuzzy set theoretic model is proposed. The uncertainties arising due to various types of imaging defects such as blurring, illumination change, noise, etc., usually result in missing of significant curvature junctions (corners). Fuzzy set theory based modeling is well known for efficient handling of impreciseness. In order to handle the incompleteness arising due to imperfection of data, it is reasonable to model image properties in fuzzy frame work for reliable decision making. The robustness of the proposed algorithm is compared with well known conventional detectors. The performance is tested on a number of benchmark test images to illustrate the efficiency of the algorithm.

Keywords: Plateaus; Multilevel; Fuzzy corners; Candidate pixels; Gradient map

1. Introduction

The human visual system has a highly developed capability for detecting many classes of patterns including visually significant arrangements of image elements. From the psychovisual aspect, points having high curvature are one of the dominant classes of patterns, that play an important role in almost all real life image analysis applications [1]. These points represent significant amount of shape information. Corners are generally formed at the junction of different edge segments which may be the meeting (or criss crossing) of two edges. Cornerness of an edge segment depends solely on the curvature formed at the meeting point of two line segments. Corner detection on gray level images can be classified into two main approaches. In the first approach, the gray level image is first converted into its binary version for extraction of boundaries using some thresholding techniques. After extraction of boundaries, the corners or the high curvature points are detected using directional codes or other polygonal approximation techniques [2].

In the second approach, the gray level image is taken as input directly for corner detection. In this paper we will restrict our discussion on the second approach only. Most of general purpose gray level corner detectors [3–8] use either topology based or auto-correlation based approach. Topology based corner detectors, mainly use gradients and surface curvature to define the measure of cornerness. Points are marked as corners, if the value of cornerness exceeds some predefined threshold condition. Alternatively a measure of curvature can be obtained using auto-correlation.

Moravec [9] developed a corner detector, in which corners are defined when there are large intensity variations in every direction. This idea is modified in Harris corner detector [10] considering the local intensity change in terms of directional derivative of surface features. It is also considered as one of the best corner detectors on gray level images. Smith and Brady proposed [11] a new method called ‘‘smallest univalue segment assimilating nucleus (SUSAN)’’, which utilize simple masking operations in place of gradient convolution. They used a circular window, to obtain USAN area, and centroid is extracted. This method has better noise robustness and localization of corners compared to other methods.

* Corresponding author. +91 3325753108; fax: +91 33257833.
E-mail addresses: minakshi_@isical.ac.in (M. Banerjee), rmalay@isical.ac.in (M.K. Kundu).

[1] Minakshi Banerjee is grateful to the Department of Science and Technology, New Delhi, India, for supporting the work under grant (SR/WOS-A/ET-111/2003).

Corner is an important feature used in various image analysis applications [12,13]. Detection of corners, using classification based approach [14,15] and fuzzy reasoning based method [16,17] both for color images [18] and gray level images is an important research issue. Real life image data are always imprecise due to inherent uncertainties that may arise from the imaging process (such as defocusing, noise, wide variations of illuminations, etc.). As a result precise localization and detection of corners became difficult under such imperfect situations. Fuzzy logic [19] can be used for possible precise measurement with imprecise data [20,21].

In this paper, we have proposed an algorithm to extract significant gray level corner points based on fuzzy set theoretic approach. The high curvature points located at the discontinuities between different uniform intensity surfaces, constitute the fuzzy corner set. The measure of cornerness varies with fuzzy edge strength and gradient direction. Different set of fuzzy corners are obtained using different values of threshold on the fuzzy edge map. The uncertainties in locating the corners points which may arise, due to discretization, noise and other imaging defects, are handled with fuzzy model. The robustness of the proposed algorithm is experimentally verified using both simulated image data and natural images, to justify the suitability of the algorithm.

The paper is organized as follows: Section 2 briefly describes the mathematical model used in this work. Section 3 describes the features extraction process. Section 4 describes the fuzzy corner extraction process. Section 5 describes the experimental results. Section 6 gives a conclusion.

2. Mathematical modeling of gray level corners

Image as fuzzy sets: an image X of size $M \times N$, with L gray levels can be considered as a fuzzy subset (A) in a space of points $X = \{x\}$ with a continuum grade of membership. Where each point in X can be characterized by a membership function $\mu_A(x_{mn})$. $A = \{(\mu_A(x_{mn})), x_{mn}\} m = 1, 2, \cdots M, n = 1, 2, \cdots N$ where $0 \leq \mu_A(x_{mn}) \leq 1.0$.

This kind of image representation is useful to handle the uncertainties arising out of gray level as well as spatial digitization [22]. A fuzzy subset (A) is defined in terms of the membership values between [0–1].

One of the most widely used mapping function to do fuzzification for converting a digital image to corresponding fuzzy subset A, is the standard S function, defined as

$$\mu_A(x) = S(x; a, b, c) = \begin{cases} 0, & x \leq a \\ 2 \times \left\{\dfrac{(x-a)}{(c-a)}\right\}^2, & a \leq x \leq b \\ 1 - 2 \times \left\{\dfrac{(x-c)}{(c-a)}\right\}^2, & b \leq x \leq c \\ 1, & x \geq c \end{cases} \quad (1)$$

with $b = (a + c)/2$

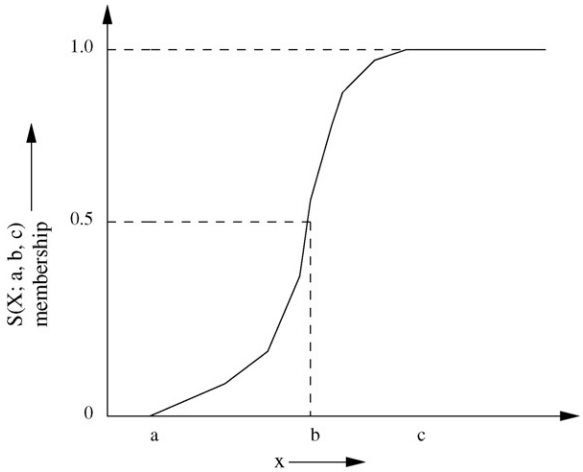

Fig. 1. S-type membership function.

Fig. 1 shows its graphical representation, where the parameter b is the cross over point, i.e., $S(b; a, b, c) = 0.5$. Similarly c is defined as the shoulder point at which $S(c; a, b, c) = 1.0$ and a is the feet point i.e. $S(a; a, b, c) = 0.0$.

fuzzy alpha cut: A fuzzy subset can be divided by suitable thresholding of membership values around the range of interest. The fuzzy alpha-cut, s_α comprises all elements of X whose degree of membership in S is greater or equal to α where

$$s_\alpha = \{x \in X : \mu_A(x) \geq \alpha\} \quad (2)$$

where $0 \leq \alpha \leq 1.0$

Plateau top, plateau bottom: In an image, edges are the transitions between two uniform intensity surfaces defined as Plateaus [23]. Let S_1 denote the set of all pixels in an image. The pixels $P, Q \in S_1$. By a plateau in S_1, is meant a maximum connected subset S_p on which the intensity (I) has a constant value. In other words $S_p \in S_1$ is a Plateau if

(i) S_p is connected. (ii) $I(P) = I(Q)$ for all $P, Q \in S_p$ (iii) $I(P) \neq I(Q)$ for all pair of neighboring points, i.e. $P \in S_p$ and $Q \notin S_p$, where $P \in S_1$ belongs to one plateau.

A Plateau S_{pt} is a top, if its gray value is a local maximum i.e. $I(P) \geq I(Q)$ for all pairs of neighboring point i.e, $P \in S_p$ and $Q \notin S_p$. Similarly we call S_{pb} a bottom, if its gray value is a local minimum. The pixels in border region B (S_{pt}, S_{pb}) can be defined as the points which are eight neighbors of at least one element of S_{pt}, S_{pb}. The pixels are labeled as pixels of a Plateau Top, Bottom and Border, considering 3×3 neighborhood [24] around each pixel.

3. Extraction of fuzzy edge map and characteristic local properties

Gray level images are inherently fuzzy in nature. Even for perfectly homogeneous objects the corresponding images will have graded composition of gray levels due to imperfection of imaging. The basic notion behind the proposed algorithm is that, a digital image can be thought of as 2D plane, where there are ridges or valleys [25,26]. This is true, when there are simply connected sequence of pixels having gray tone intensity values

significantly higher (lower) in the sequence than the neighboring pixels. Desired features can therefore be obtained by extracting and assembling topographic characteristics of intensity surfaces.

The basic assumption is that, corner points are high curvature points and should lie on gray level edges. It should have significant change in edge direction with linear arm support of considerable length on both sides.

3.1. Feature extraction

The feature computation process consists of two phases. In the first phase, the possible candidate edge pixels (P_c) are extracted from the border regions between the uniform intensity surfaces, as explained in the earlier section, which are defined in terms of Plateau Top and Bottom. These are similar to ridges and valleys of gray level images. The edge candidates (P_c), which belong to the border regions are assigned gradient membership $\mu_c(P)$ [27] based on their respective gradient strength. A fuzzy edge set (e_d) comprising of $\mu_c(P)$ for the border points $P \in P_c$ is formed, as defined in (3). In the next step, two membership functions ($\mu_f(P)$ and $\mu_b(P)$) are computed to estimate the fuzzy connectivity strength along a path, in the forward and backward direction with respect to the candidate pixel. The basic steps are explained in Fig. 2. The detailed implementation of the steps are described in the following subsections.

$$e_d = \{(\mu_c(P), P_c)\} \tag{3}$$

3.2. Estimation of gradient strength $\mu_c(P)$

The input image $I(m,n)$ is convolved with the Gaussian function, to obtain the Gaussian smoothened image matrix $I_b(m,n)$.

$$I_b(m,n) = I(m,n) * G(m,n) \tag{4}$$

$G(m,n) = (1/\sqrt{2}\pi\sigma)e^{-}(m^2+n^2)/2\sigma^2$ where σ effectively determines the degree of smoothing.

Gaussian filtering, has been chosen to perform effective smoothing of small distortions caused by noise and to obtain blur boundaries. The size of the Gaussian smoothing filter is fixed to 3×3 pixels and value of σ to 1.5.

The membership $\mu_c(P)$ for the pixels $P \in P_c$ are estimated as follows.

For every edge pixel $P(p_i)$ where p_i is the gray value of pixel (P), a 3×3 window is considered as shown in Fig. 3. In Fig. 3 the symbols represent the gray values at different neighborhoods of P. The difference between (a_1, a_2), (c_1, c_2), (b_1, b_2), (d_1, d_2) are taken as gray level differences in four

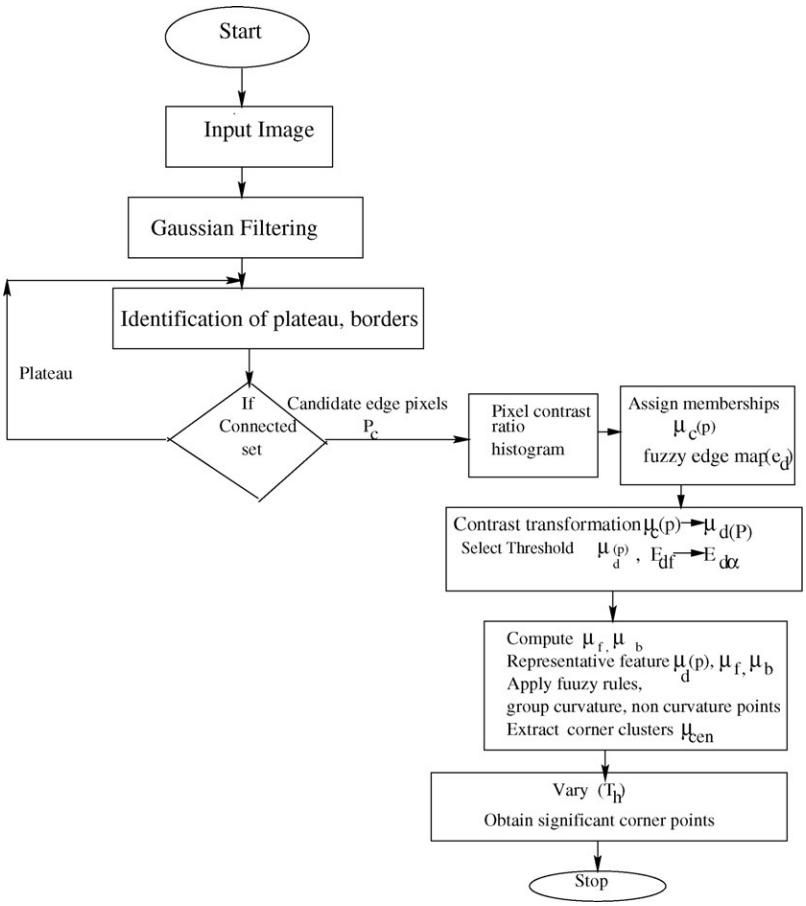

Fig. 2. Block diagram of the proposed algorithm.

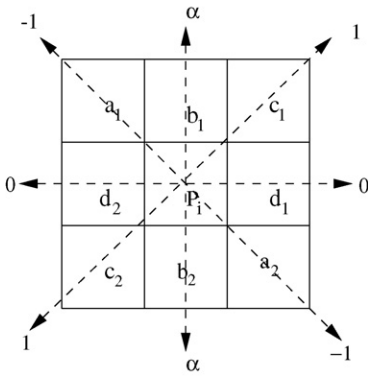

Fig. 3. 3×3 neighborhood of a pixel.

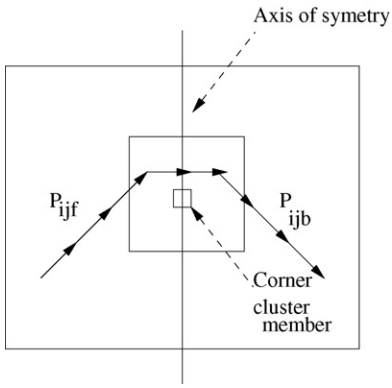

Fig. 4. Determination of cornerness.

different directions. The ratio of gray label changes (X_r) are computed from two mutually perpendicular set of pixel pairs within the neighborhood. Considering the mutually perpendicular pair $(a_1\, p_i a_2)$, $(c_1\, p_i c_2)$, the computed ratios are, $1 + |a_1 - a_2|/1 + |c_1 - c_2|$, $1 + |c_1 - c_2|/1 + |a_1 - a_2|$ [27]. Similarly, $(b_1\, p_i b_2)$, $(d_1\, p_i d_2)$ are considered. The four values of pixel contrast ratios (X_r) as obtained from the neighborhood of each candidate edge pixel are shown in (5).

$$X_r = \left[\frac{1 + |a_1 - a_2|}{1 + |c_1 - c_2|}, \frac{1 + |c_1 - c_2|}{1 + |a_1 - a_2|}, \frac{1 + |b_1 - b_2|}{1 + |d_1 - d_2|}, \frac{1 + |d_1 - d_2|}{1 + |b_1 - b_2|}\right] \tag{5}$$

In a window of eight neighborhood, an edge pixel will have maximum gray level difference in a direction, perpendicular to its true edge direction (ϕ). The edge direction (ϕ) should point along the minimum difference direction [28]. The minimum pixel contrast ratio ($X_m r$),

$$X_m r = \min\{X_r\} \tag{6}$$

is the parameter (x) used for computing the gradient membership $\mu_c(P)$ with a S type function, as shown Eq. (1). $\mu_c(P)$ is used to represent the uncertainties of edge strength and location of true edge point.

The choice of membership function is problem dependent. Here a monotonic type S function has been chosen for suitable representation of the ambiguities of the set, computed from pixel contrast ratios. We have computed the feet and the shoulder point using $\max(X_m r)$ and $\min(X_m r)$ values of the contrast ratios ($X_m r$), over which the membership $\mu_c(P)$ is computed. The histogram plots of pixel contrast ratio are shown in Fig. 6(a) and (b) for the images Fig. 5 (a) and (b) respectively.

The value of $\mu_c(P)$ determines the edge strength. Higher values of gradient memberships, i.e. $\mu_c(P) \geq 0.5$ correspond to medium and strong edge points. Lower values of $\mu_c(P)$ correspond to weak or noisy edge points.

The fuzzy gradient map (e_d) as shown in (3) is obtained.

3.3. Estimation of connectivity strength $\mu_f(P)$ and $\mu_b(P)$

The two membership values ($\mu_f(P)$ and $\mu_b(P)$) are computed on a selected subset of (e_d) shown in (3) obtained by thresholding (e_d). The memberships $\mu_f(P)$ and $\mu_b(P)$ are computed from the difference in edge directions between the connected pixels within a fixed window. The actual computation of $\mu_f(P)$ and $\mu_b(P)$ are made as follows:

Let $\phi = \{\phi_1, \phi_2, \ldots \phi_n\}$ represent the edge direction of a sequence of pixels on an edge segment. The present approach, deals with the changes in edge directions. Four relative (the angle subtended between two successive pixels), directions are considered in a 3×3 window.

The directions (ϕ) along the horizontal line i.e. (0° and 180°) are labeled as (0), similarly along the vertical lines as (∞) and along the diagonal lines as $(+1, -1)$ as shown in Fig. 3. As a result, the edges along different directions may be labelled as shown in (7).

$$A_{df} \in \{0, 1, \infty, -1\} \tag{7}$$

The change of directions with respect to (ϕ) between the successive edge pixels may have values $(\phi + \pi/4)$, $(\phi - \pi/4)$, $(\phi + \pi/2)$, $(\phi - \pi/2)$ in an eight neighborhood. However due to blurring of the images, the sharp changes like $(\phi + \pi/2)$, $(\phi - \pi/2)$ between the successive pixels are converted to gentle changes having values less than $\pi/2$. As a result, the changes at a step of 45° are considered.

If the direction of the candidate pixel P is ϕ, then $\phi_f = \phi + \pi/4$ is considered as relative forward direction and $\phi_b = \phi - \pi/4$ is considered as the relative backward direction with respect to ϕ. A $m \times m$ window is centered around the selected candidate edge pixels and the number of simply connected edge pixels of (e_d) which have directions ϕ_f and ϕ_b are counted. If the label of ϕ is (0) then, the labels $(1, -1)$ represents the counts n_f and n_b respectively. Similarly if the label of ϕ is (1), the labels $(\infty, 0)$ represent the counts n_f and n_b respectively and so on.

This count is expected to vary with the sharpness of the curvature type. The values ($\mu_f(P)$, $\mu_b(P)$) are represented with the form of membership function,

$$\mu_f(P) = K * \exp(-x) \tag{8}$$

where $x = \frac{1}{n_f}$,

Similarly μ_b is defined by

$$\mu_b(P) = K * \exp(-x) \tag{9}$$

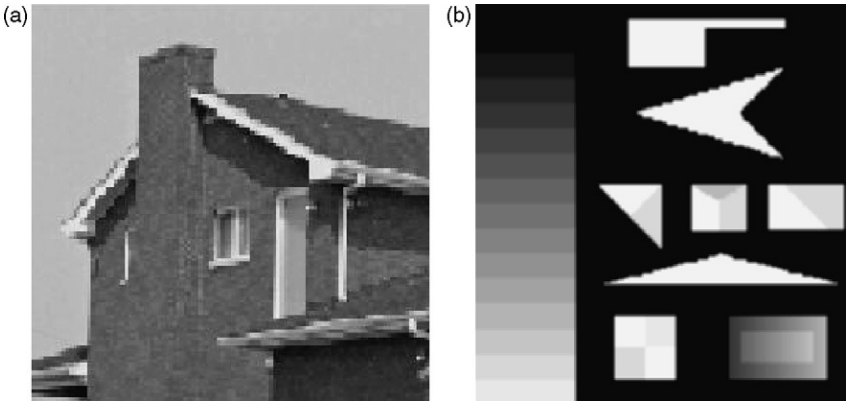

Fig. 5. (a)Original image of house. (b) Image having prominent curvature junctions.

where $x = 1/n_b$, K is a constant multiplier. It is so selected that the value of $\mu_f(P)$ or $\mu_b(P)$ should lie in between 0 and 1.0 from the finite counts of n_f and n_b of the image.

Each candidate edge pixel (P) selected for cornerness testing, is thus represented by a three-dimensional feature vector F_i where,

$F_i = [\mu_c(P), \mu_f(P), \mu_b(P)]$. Detection of possible fuzzy corners from the input edge map (e_d) will be discussed in the next section.

4. Multilevel fuzzy corner extraction

The fuzzy edge map (e_d) is represented as set of points $\{(\mu_c(P), P_c)\}$. In the initial stage, a suitable threshold value of gradient membership, has to be decided to select a subset $E_{d\alpha}$ of e_d, and only those points are used for computation of, $\mu_f(P)$, $\mu_b(P)$ for detection of fuzzy corners.

4.1. Membership transformation

Any natural image consists of different homogeneous regions, where the shape of each region is characterized by its bounding lines. But in many practical situations the boundaries are so faint that it becomes difficult to distinguish between two regions. Moreover due to noise and non uniform illumination, spurious edges may also appear. It is also difficult to discriminate between spurious edges and weak edges. Under such situation, the gradient information (both edge strength, and direction information) may be required to cut of where $\mu_c(P)$ is very small. To locate points from significant portions on the image, a contrast transformation may be used as a preprocessing step. The extraction of probable edge candidates, is achieved by thresholding through non-linear transformation of membership values $\mu_c(P)$ such that, the points having values greater than 0.5 are stretched and those below 0.5 are squeezed.

$$E_{df} = T'(e_d) \tag{10}$$

A pixel contrast transformation operation [22] is represented in (11)

$$\mu_d(P) = \begin{cases} 2 \times \mu_c(P)^2, & 0 \le \mu_c(P) \le 0.5 \\ 1 - 2 \times (1 - \mu_c(P))^2, & 0.5 \le \mu_c(P) \le 1.0 \end{cases} \tag{11}$$

The results before and after transformation of membership values are shown in Fig. 7 (a)–(c). As seen from Fig. 7(a),(b) the number of insignificant candidate points are reduced at the same threshold value. Thresholding the transformed edge map ($E_{df} = \{\mu_d(P), P\}$) above different membership values may be obtained by using proper (α-cuts) [22] as mentioned in section 2. As a result, we obtain the edge maps $E_{d\alpha}$ at different levels

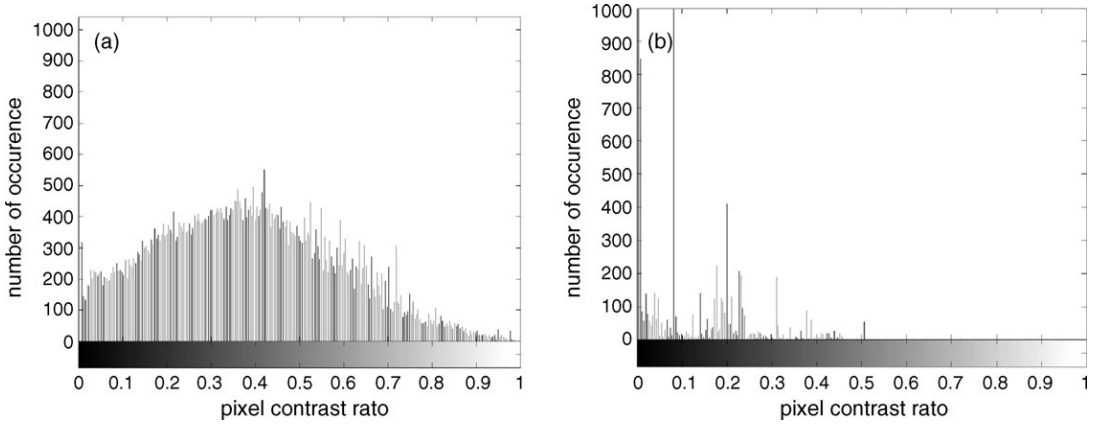

Fig. 6. (a) Pixel contrast histogram of: Fig. 5(a). (b) Pixel contrast histogram of Fig. 5(b).

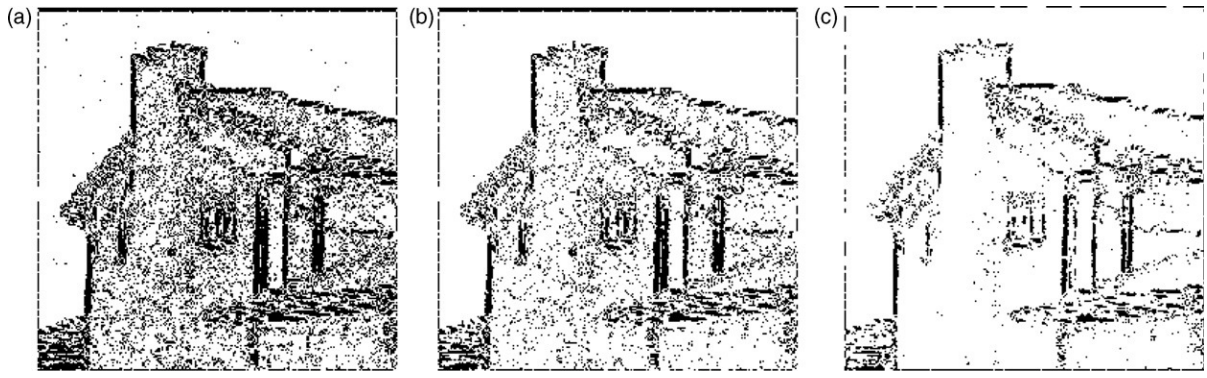

Fig. 7. Fuzzy edge map: (a) ($\mu_c(P) \geq 0.4$). (b) ($\mu_d(P) \geq 0.4$) after membership transformation. (c) ($\mu_d(P) \geq 0.9$).

from E_{df}, as shown in (12).

$$E_{d\alpha} = \{P \in E_{df} : \mu_d(P) \geq \alpha\} \tag{12}$$

where $0 \leq \alpha \leq 1.0$ The candidates of $E_{d\alpha}$ can be represented by the local features $F_{if} = [\mu_d(P), \mu_f(P), \mu_b(P)]$.

By such thresholding of E_{df}, multilevel fuzzy edge maps may be generated, where the pixels may be segregated as (strong, medium, weak) edge pixels based on their gradient membership values $\mu_d(P)$ as shown in Fig. 10 (b)–(d). If the local contrast of a region is very poor, then $\mu_d(P)$ values of different edge points are very close to each other. Ambiguity in locating curvature points in these regions may increase due to close proximity of values of different points, as seen in the bottom rectangle of Fig. 10(b). On the other hand, the membership values of different points are widely separated above the cross over points ($\mu_d(P) \geq 0.5$), where the local contrast is better resulting in less ambiguity.

In the transformed set, points having ($\mu_d(P) \geq 0.5$) will include edge points with higher and medium strength. Whereas those having values ($\mu_d(P) \geq 0.0$) may select lot of spurious edge points along with high and medium type of curvature points.

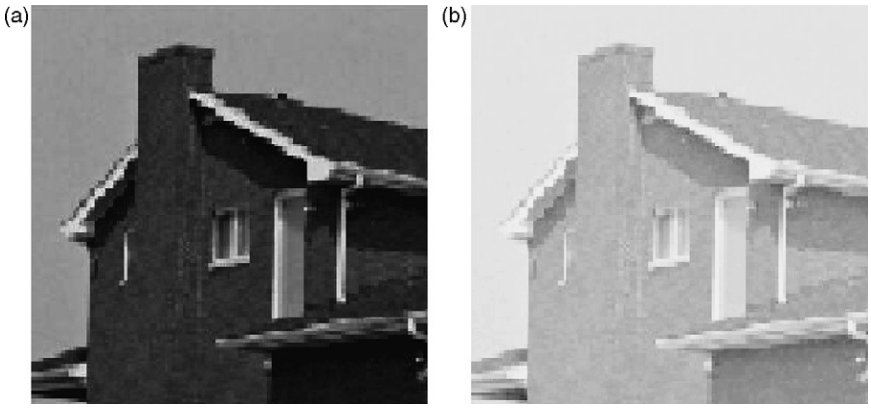

Fig. 8. Image of house: (a) underexposed, (b) overexposed.

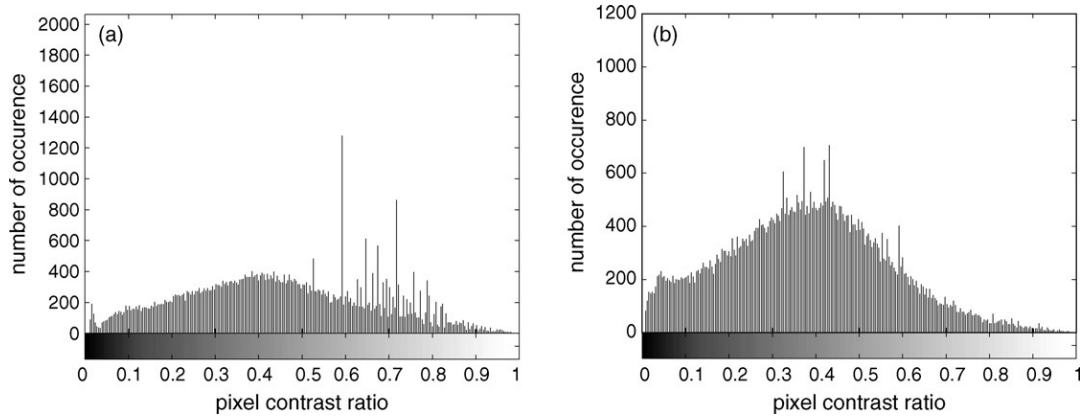

Fig. 9. Histogram plots of image of house: (a) underexposed, (b) overexposed.

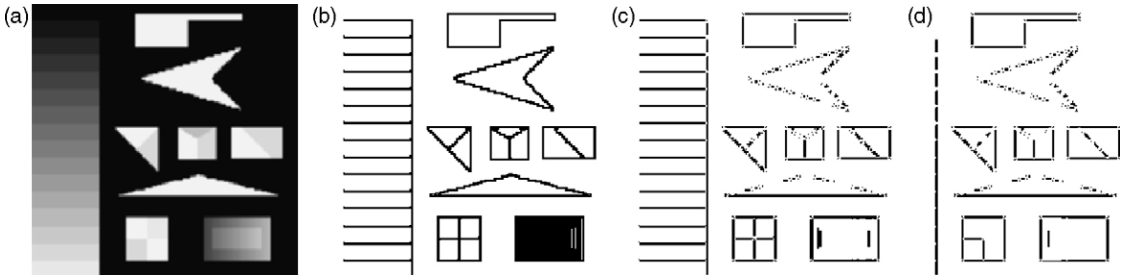

Fig. 10. (a) Original image. (b) Edge image for ($\mu_d(P) > 0.0$). (c) ($\mu_d(P) \geq 0.6$). (d) ($\mu_d(p) \geq 0.9$). Points above threshold are plotted as crisp edge points.

Thus a proper choice of threshold ($\mu_d(P)$) selection is necessary, below which the variations are considered to be noise.

4.2. Selection of threshold on membership value

The gradient membership value $\mu_d(P)$ used for thresholding the edge map, is decided from the pixel contrast ratio histogram.

The histogram of contrast ratio gives an estimate of global description of the appearance of an image.

In general, the choice of threshold is made as follows:

A higher threshold value, typically $\mu_d(P) \geq 0.8$ is chosen, to reduce the false acceptance rate, if the nature of the contrast histogram is as follows: (i) The contrast histogram occupies most of the histogram levels, which are in contiguous locations. (ii) The number of occurrences for each ($X_m r$) value is quite close and covers the majority of the total dynamic range. This is seen from the histogram plots of Figs. 5(a) and 8(a), (b).

As we are concerned with the dynamic range, and not the absolute gray scale values, such thresholding can be applied for almost all natural images, even undergone varying imaging conditions like overexposed, underexposed, blurred etc. The contrast histogram plot for Fig. 8(a) and (b) are shown in Fig. 9(a) and (b).

On the other hand a lower threshold value of $\mu_d(P)$, typically $\mu_d(P) > 0.0$ is chosen, if the histogram has the following properties. (i) Sparsely distributed contrast levels. (ii) Having widely different occurrences for different ($X_m r$) values (iii) Does not cover majority of the dynamic range. Such cases may arise for nearly binary images as seen in, Fig. 5(b) and Fig. 19. In such cases transformation of $\mu_c(P)$ to $\mu_d(P)$, does not affect the results much, as the candidate weak edges are less in number.

This has been tested over number of images and the strategy described is found to be satisfactory.

4.3. Estimation of local shape parameters

Once the suitable threshold value of $\mu_d(P)$ is chosen, the next task is to categorize the edge pixels based on the local properties estimated from $\mu_f(P)$ and $\mu_b(P)$. The selected edge candidates constitute the points of $E_{d\alpha}$ for which the membership values $\mu_f(P)$, $\mu_b(P)$ are computed. The properties of $\mu_f(P)$, $\mu_b(P)$ are used to examine local shape parameters, which are defined as straightness and cornerness. Properties of $\mu_f(P)$ and $\mu_b(P)$ for any of the selected points (P) on the edge map is shown in Table 1.

Straightness: This property is determined by comparing pixels translated along the direction of edge. It is expected that a pixel translated in the direction of straight edge will be connected to pixels of same direction. Hence $\mu_f(P)$ and $\mu_b(P) \simeq 0.0$.

Cornerness: This property is determined from comparing pixels having reflexive symmetry. The pixels are expected to be reflected from one arm to the other on both sides of the curvature junction within the region of evaluation, as shown in Fig. 4.

The points of $E_{d\alpha}$ as shown in Eq. (12) having both $\mu_f(P)$ and $\mu_b(P)$ equal to zero can be filtered out as the non corner pixels. As a result the interesting regions constituting a group of curvature points of the fuzzy edge image can be separated. We attempt to approximate this region with a quantitative measure by exploiting the properties of $\mu_f(P)$ and $\mu_b(P)$.

The pixels in the proximity of the curvature junction as shown in Fig. 4 can be categorized from the following rules, (i) The points with $\mu_f(P)$ high and $\mu_b(P)$ low constitute the points on the left side of the junction point. We designate these points as P_{ijf}, (as shown in Fig. 4) on forward arm and assign membership $\mu_f(P) - \mu_b(P)$. This difference is expected to vary with the sharpness of curvature. The points of P_{ijf} represent a fuzzy subset as μ_{fram}.

$$\mu_{fram}(P) = \mu_f(P) - \mu_b(P) \tag{13}$$

(ii) The points with $\mu_b(P)$ high and $\mu_f(P)$ low constitute the points on the right side of the junction point. We designate these points as P_{ijb}, (as shown in Fig. 4) on backward arm and assign membership μ_b- μ_f. The points of P_{ijb} represent a fuzzy set μ_{bram}.

$$\mu_{bram}(P) = \mu_b(P) - \mu_f(P) \tag{14}$$

Table 1
Fuzzy cornerness measure

$\mu_f(P)$	$\mu_b(P)$	Cornerness	Straightness	Location
High	Low	High	Low	Forward arm
High	High	High	Low	Near curvature junction
Low	High	High	Low	Backward arm
Low	Low	Low	High	Straight edge

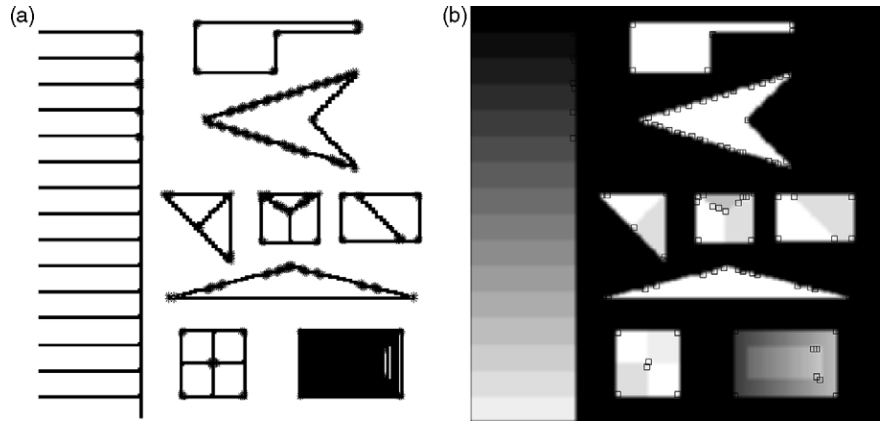

Fig. 11. (a) Curvature points (*), ($\mu_d(P) > 0.0$ and $T_h = 0.1$). (b) Representative point of each cluster.

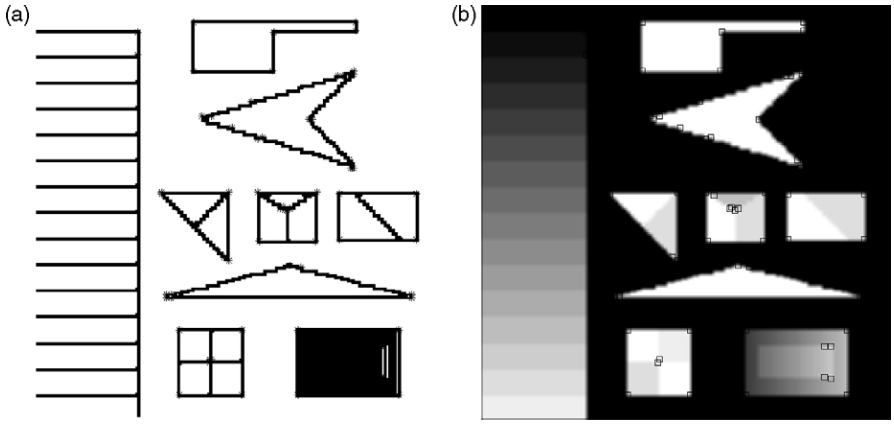

Fig. 12. (a) Curvature points (*), ($\mu_d(P) > 0.0$ and T_h=0.2). (b) Representative points of each cluster.

(iii) The points very near to the junction is expected to have high or medium values of $\mu_f(P)$ and $\mu_b(P)$.

Having obtained the two fuzzy sets, μ_{fram} and μ_{bram}, a third fuzzy subset μ_{cen} which is surrounded by both μ_{fram} and μ_{bram} lie approximately on the axis of symmetry. This region constitute the ambiguous corners. The cluster of such points (*) represented as μ_{cen} are shown in Figs. 11(a), 12(a), 13(a) and 14(a) respectively. The points belonging to μ_{cen} are those points, having other points with $\mu_{fram}(P) > 0$ and $\mu_{bram}(P) > 0$ in the neighborhood of fixed window size.

The extracted curvature points may be of different sharpness type (sharp, medium, weak). The characteristics of sharp curvature points will be confined within a small region but for that of medium and weak type the region will be larger. In view of the above facts, we use a measure T_h that controls the shape and size of the extracted μ_{cen}.

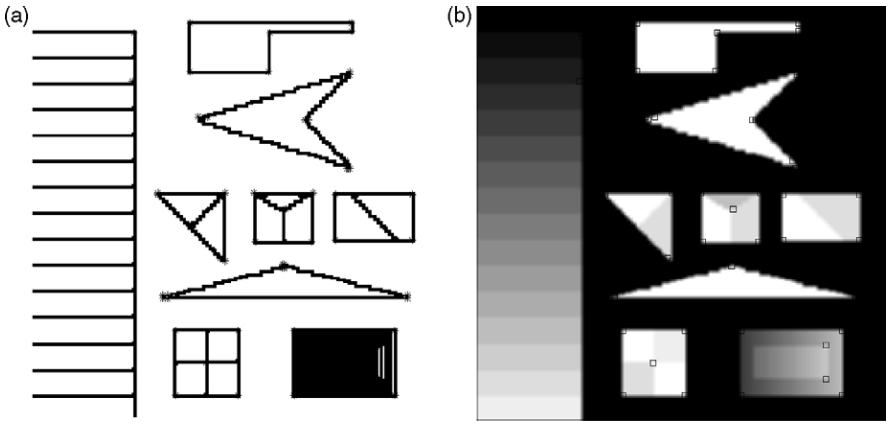

Fig. 13. (a) Curvature points (*), ($\mu_d(P) > 0.0T_h$=0.3). (b) Representative points of each cluster.

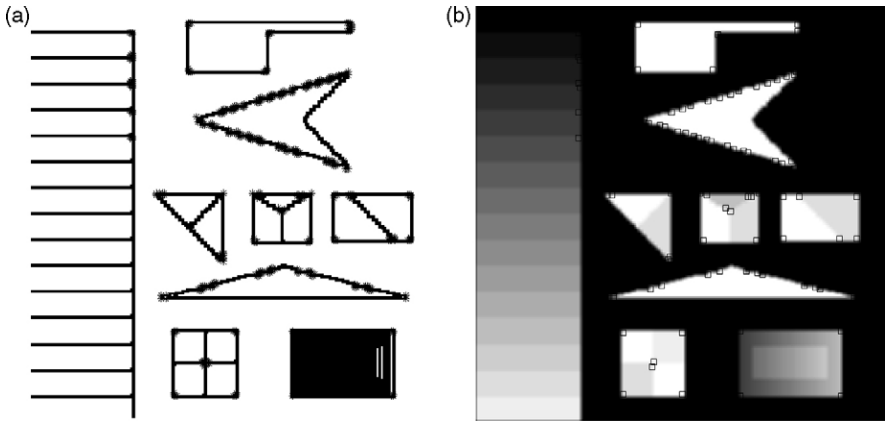

Fig. 14. (a) Curvature points (*), ($\mu_d(P) > 0.6$ and T_h =0.1). (b) Representative point of each cluster.

In order to define a quantitative measure of the region, constituting of points of μ_{cen}, we compute the sum total of differences for all the pairs of μ_{fram} and μ_{bram} which fall within the region of evaluation, a nxn window. This value is subtracted from a large value y_{max} (kept fixed at 2.0, found experimentally better) to make it increase with sharpness.

$$T_h = y_{max} - \sum_{i=-n/2}^{j=n/2} \sum_{i=-n/2}^{j=n/2} \mu_{fram} - \mu_{bram} \quad (15)$$

The representative points i.e., the cluster center of each localized region (μ_{cen}) is represented by C_{ij} whose coordinate is equal to the average value of the co-ordinates of the n points of each cluster as shown in Figs. 11(b), 12(b), 13(b) and 14(b). $C_{ij} = [\sum x_j/n, \sum y_j/n]$.

At fixed value of $\mu_d(P)$ the value of T_h is experimentally varied from (0.1-0.3) to generate corners of different sharpness.

Computational complexity: The analysis of the computational complexity (worst case) involved in different operations for an image of size $M \times M$ and with window neighborhood $N \times N$, is explained as follows: (1) Identification of border regions require M^2N^2 operations. (2) Computation of pixel contrast ratio involves λM^2N^2 operations (where $0 < \lambda < 1.0$). (3) Assignment of $\mu_c(P)$ involves λM^2 operations. (4) Membership transformation involves λM^2 operations. (5)

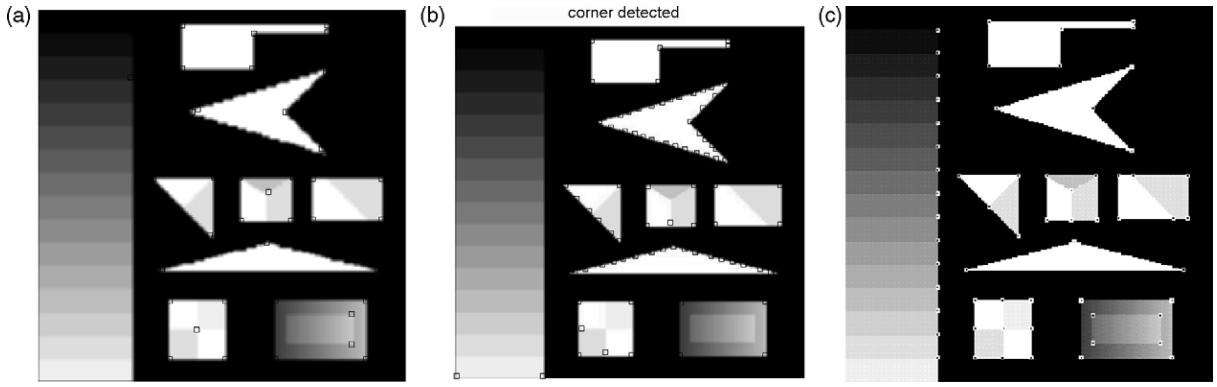

Fig. 15. Corner points (a) Our detector ($\mu_d(P) > 0.0T_h$=0.3). (b) Harris detector (c) SUSAN.

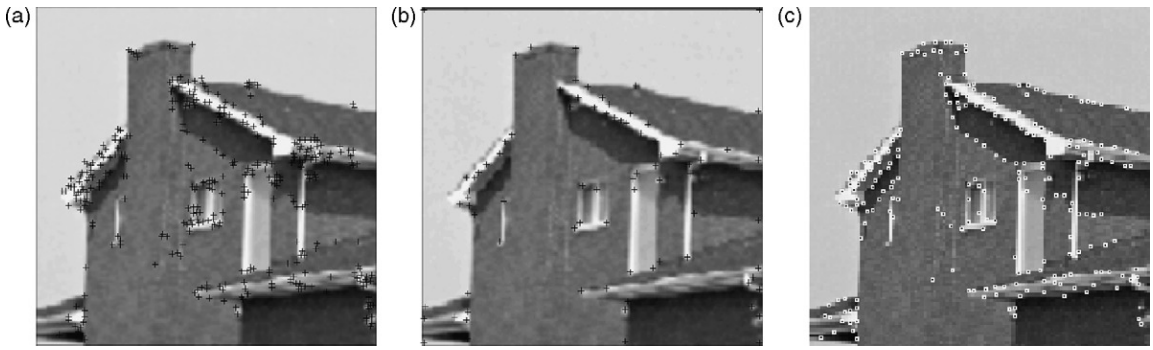

Fig. 16. Corner points (a) Our detector ($\mu_d(P) \geq 0.9$ and T_h=0.2). (b) Harris detector (c) SUSAN.

Thresholding involves λM^2 operations. (6) Computation of μ_f and μ_b involves λM^2N^2 operations. (7) Grouping of pixels based on fuzzy rules involves λM^2 operations. (8) Computation of T_h involves λM^2N^2 operations. The total operation is of the order of O (M^2N^2).

5. Experimental results

We have examined the performance of our detector on various type of images including images which have undergone image alterations like blurring, illumination change, noise etc. Image as shown in Fig. 10(a) contains objects of different shapes with varying illumination. The procedure involves extraction of edge map. The edge map of Fig. 10(a) are thresholded above different membership values as shown in Fig. 10(b)–(d) for ($\mu_d(P) \geq 0.0$), ($\mu_d(P) \geq 0.6$), ($\mu_d(P) \geq 0.9$), respectively. The points above the threshold values are represented as dark edge pixels. It is to be noted that the internal structure of the rectangle (represented as dark region) shown in Fig. 10(b) could not be extracted properly due to poor

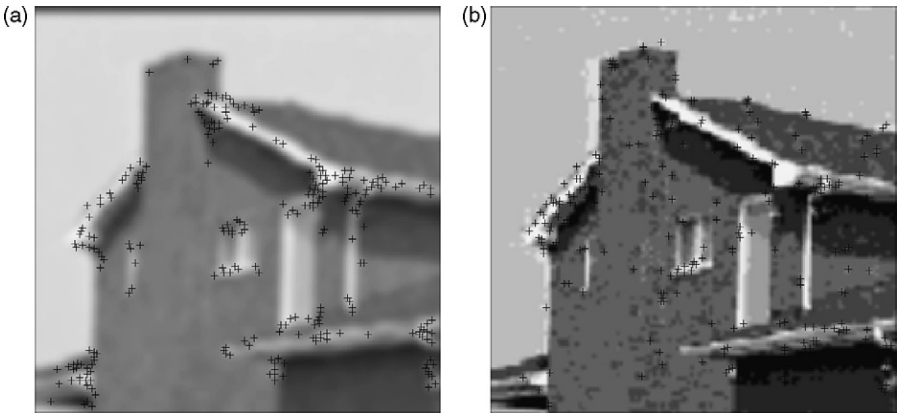

Fig. 17. Corner points from our detector (a) blurred image ($\mu_d(P) \geq 0.9$ and T_h=0.2. (b) noisy image.

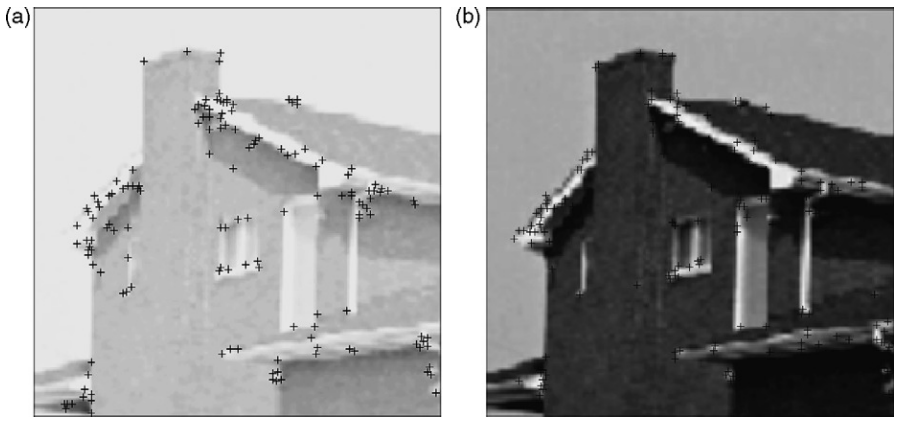

Fig. 18. Corner points under illumination change: (a) Overexposed ($\mu_d(P) \geq 0.9$ and T_h=0.3). (b) Underexposed case ($\mu_d(P) \geq 0.9$ and T_h=0.3).

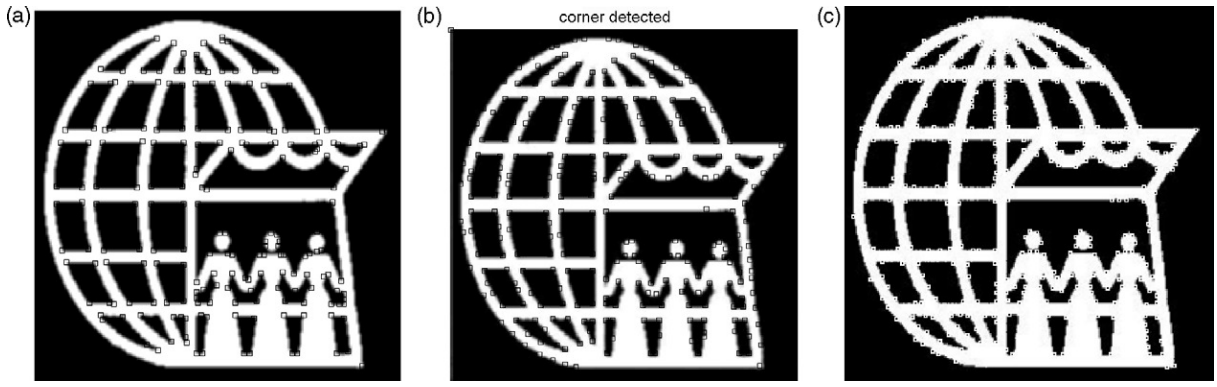

Fig. 19. Corner points (a) Our detector($\mu_d(P) > 0.0$ and T_h=0.2). (b) Harris detector. (c) SUSAN.

contrast between the two regions. In such cases, the extraction of the structure could not be done properly as the gradient value of the edge pixels are very low and the threshold is ($\mu_d(P) \geq 0.0$). At a higher threshold value of $\mu_d(P)$, stronger edge points mainly representing the boundary points can easily be separated as shown in Fig. 10(d). The curvature points of various regions are depicted by symbol '*' as shown in Figs. 11(a), 12(a), 13(a) and 14(a). The representative point from each cluster is shown in Figs. 11(b), 12(b), 13(b) and 14(b). The different type of curvature points are obtained by varying T_h and $\mu_d(P)$ and shown in Figs. 11(b), 12(b) and 13(b). The results of our algorithm are comparable to that of most popularly used corner detectors like Harris and SUSAN detector and are shown in Figs. 15 and 16. The performance of different corner detectors varies with the type of the image and to obtain the best results, several parameters need to be adjusted for almost all detectors. We have tried to compare our results with the best results obtained from each detector with the parameter values as suggested by authors. In our algorithm better results are obtained by keeping the threshold of $\mu_d(P)$ at a lower value when there are lesser number of gray level variations e.g., Fig. 5(b). On the other hand when there are large variations of distinct gray values as that of Fig. 5(a), higher threshold value of $\mu_d(P)$ is chosen to reduce the number weak and noisy edge points. Such results are shown in Figs. 16–18. It is seen from Fig. 15(a)–(c) that the corner points obtained by our method shown in Fig. 15(a) is quite comparable to that of Harris shown in Fig. 15(b) and SUSAN detector in Fig. 15(c). However SUSAN is able to extract corners from very low contrast area. The results on the house image with threshold value ($\mu_d(P) \geq 0.9$ and $T_h = 0.2$) for our algorithm, for Harris and SUSAN method are shown in Fig. 16(a)–(c), respectively. It is seen from Fig. 16 that the corner points obtained by our method shown in Fig. 16(a) is comparable to that of Harris in Fig. 16(b) and SUSAN in Fig. 16(c). Our result is closer to that of SUSAN with some more details of curvature information that exists in different regions of the house image. The results obtained under different imaging conditions are shown from Figs. 17 and 18. It is to be noted that our proposed detector is able to extract most of significant structural corner points under varying imaging conditions. This is due to the fact that the slope of the fuzzy property plane is determined from the dynamic range. Although the gray level contrast information is reduced in the over exposed case in Fig. 18, but due to additional contrast intensification, significant edge pixels are selected above threshold for cornerness detection. Even for nearly binary images our algorithm works satisfactorily as seen from Fig. 19(a)–(c).

6. Conclusion

A fuzzy set theoretic approach for detection of corners is proposed in this paper. The proposed algorithm does not require computation of chain codes or complex differential geometric operators. Experiments have been performed on various types of images to illustrate the efficiency of our algorithm. The algorithm performs reasonably well under different imaging conditions. However we intend to improve the algorithm, so that the parameters may be selected adaptively for thresholding. Significant features computed from these dominant high curvature fuzzy points can be used directly for indexing an image for image retrieval purpose.

References

[1] D.G. Lowe, Perceptual Organization and Visual Recognition, Kluwer Academic Publishers, USA, 1985.
[2] H. Freeman, L.S. Davis, A corner-finding algorithm for chain-coded curves, IEEE Trans. Comput. C-26 (1977) 297–303.
[3] L. Kitchen, A. Rosenfeld, Gray-level corner detection, Pattern Recogn. Lett. 1 (1982) 95–102.
[4] Z. Zheng, H. Wang, E. Teoh, Analysis of gray level corner detection, Pattern Recogn. Lett. 20 (2) (1999) 149–162.
[5] A. Rattarangsi, R.T. Chin, Scale-based detection of corners of planar curves, IEEE Trans. Pattern Anal. Mach. Intell. 14 (4) (1992) 430–449.
[6] C. Teh, R.T. Chin, On the detection of dominant points on digital curves, IEEE Trans. Pattern Anal. Mach. Intell. 11 (8) (1989) 859–872.
[7] A. Rosenfeld, E. Johnston, Angle detection on digital curves, IEEE Transaction on Computers C-22 (1973) 858–875.
[8] S.C. Bae, I.S. Kweon, C.D. Yoo, Cop: a new corner detector, Pattern Recogn. Lett. 20 (2002) 1349–1360.
[9] H. Moravec, Towards automatic visual obstacle avoidance, in: Proceedings of the 5th International Joint Conference on Artificial Intelligence, 1997, p. 584.
[10] C. Harris, M. Stephens, A combined corner and edge detector, in: Proceedings of the 4th Alvey Vision Conference, 1988, pp. 147–151.
[11] S. Smith, M. Brady, A new approach to low level image processing, Int. J. Comput. Vision 23 (1) (1997) 45–78.
[12] E. Loupias, N. sebe, Wavelet-based salient points: applications to image retrieval using color and texture features, in Advances in visual Information Systems, in: Proceedings of the 4th Intenational Conference, VISUAL 2000, (2000), pp. 223–232.
[13] M. Fischler, H.C. Wolf, Locating perceptually salient points on planar curves, IEEE Trans. Pattern Anal. Mach. Intell. 16 (2) (1994) 113–129.
[14] M. Banerjee, M.K. Kundu, P. Mitra, Corner dectection using support vector machine, in: 17th International Conference on Pattern Recognition ICPR(2004), UK, vol. 2, (2004), pp. 819–822.
[15] K.J. Lee, Z. Bien, A gray-level corner detector using fuzzy logic, Pattern Recogn. Lett. 17 (1996) 939–950.
[16] L. Li, W. Chen, Corner detection and interpretation on planar curves using fuzzy reasoning, IEEE Trans. Pattern Anal. Mach. Intell. 14 (4) (1999) 1204–1209.
[17] T. Law, H. Itoh, H. Seki, Image filtering, edge detection and edge tracing using fuzzy reasoning, IEEE Trans. Pattern Anal. Mach. Intell. 18 (5) (1996) 481–491.
[18] J. Weijer, T. Gevers, J. Geusebroek, Edge and corner detection by photometric quasi-invariants, IEEE Trans. Pattern Anal. Mach. Intell. 27 (4) (2005) 625–629.
[19] L.A. Zadeh, Fuzzy sets, Information and Control 8 (1965) 338–353.
[20] S.K. Pal, A. Ghosh, M.K. Kundu, Soft Computing for Image Processing, Physica-Verlag, 2000, pp. 44–78 (Chapter 1).
[21] D. Yua, Q. Hu, C. Wua, Uncertainty measures for fuzzy relations and their applications, Appl. Soft Comput. 7 (3) (2007) 1135–1143.
[22] S.K. Pal, D.D. Majumder, Fuzzy mathematical Approach to Pattern Recognition, John Willey, New York, 1985.
[23] A. Rosenfeld, Fuzzy digital topology, in: J.C. Bezdek, S.K. Pal (Eds.), Fuzzy Models For Pattern Recognition, IEEE Press, 1991 , pp. 331–339.

[24] B.B. Chaudhury, B.U. Shankar, An efficient algorithm for extrema detection in digital images, Pattern Recogn. Lett. 10 (1989) 81–85.
[25] L. Wang, T. Pavlidis, Direxť gray-scale extraction of features for character recognition, IEEE Trans. Pattern Anal. Mach. Intell. 15 (10) (1993) 1053–1066.
[26] R.M. Haralick, Ridges and valleys on digital images, Computer Vision, Graphics Image Process. 22 (1983) 28–38.
[27] M. Banerjee, M.K. Kundu, Edge based features for content based image retrieval, Pattern Recogn. 36 (11) (2003) 2649–2661.
[28] R.C. Gonzalez, R.E. Woods, Digital Image Processing, Addison Wiley, New York, 1985.